INTERNATIONAL JOURNAL FOR NUMERICAL METHODS IN FLUIDS, VOL. 12, 125–142 (1991)

FINITE DIFFERENCE SOLUTION OF A NEWTONIAN JET SWELL PROBLEM

TA-JO LIU*, TSAI-AN YU AND SHU-HUE CHENG

Department of Chemical Engineering, National Tsing Hua University, Hsinchu, Taiwan 30043, R.O.C.

SUMMARY

A finite difference technique has been developed to study the Newtonian jet swell problem. The streamfunction and vorticity were used as dependent variables to describe the jet flow. The boundary-fitted co-ordinate transformation method was adopted to map the flow geometry into a rectangular domain. The standard finite difference method was then applied for solving the flow equations. The location of the jet free surface was updated by the kinematic boundary condition, and an adjustable parameter was included in the free-surface iteration. We could obtain numerical solutions for the Reynolds number as high as 100, and the differences between the present study and previous finite element simulations on the jet swell ratio are less than 5%.

KEY WORDS Jet swell Finite difference method

INTRODUCTION

The phenomenon of jet swell appears in many industrial applications, and an accurate theoretical description of the fluid-swelling behaviour will be helpful for these operations.[1] Numerical solution of the jet swell problem is difficult because it is necessary to locate the free surface of the jet as part of the solution. The jet swell problem has become a popular test case for free-surface flow simulations. Several numerical techniques for solving the jet swell problem were recently reviewed by Tanner,[2] and the strategy for locating the free surface was discussed in detail by Kistler.[3] The finite element method has been well developed for simulating the jet flow accurately, and the range of applicability has been extended to the cases of high Reynolds number and high surface tension;[4] whereas for the finite difference method the development has been slow and rare. Early works using the finite difference method led to erroneous results;[2] only recently did Dutta and Ryan[1] overcome the difficulty of locating the free surface of the jet by using an orthogonal mapping technique to transform the flow geometry into a rectangular domain, and they solved the flow problem of a creeping Newtonian jet successfully.

Since the finite difference method has its merits—such as the formulation and mesh refinement are easy,[1] time discretization for both the finite difference and finite element methods is usually based on the finite difference method,[5] and extension of finite difference simulation for steady flow problems to time-dependent problems can be carried out in a straightforward manner—it is useful to develop an efficient numerical scheme for treating free-surface flow problems. This is our

* To whom correspondence should be addressed.

0271–2091/91/020125–18$09.00

Received 2 August 1989
Revised 27 February 1990

motivation and we have developed a finite difference scheme for solving the planar Newtonian jet swell problem.

We take a similar approach to that of Dutta and Ryan, i.e. the mathematical problem is formulated with streamfunction and vorticity as dependent variables and a mapping technique is applied so that the flow problem is solved in a transformed plane. However, we have adopted a more flexible mapping technique, the boundary-fitted co-ordinate transformation method (BFCTM) developed by Thompson *et al.*,[6,7] and we have found that it is necessary to have an adjustable parameter in the free-surface iteration for the cases of non-zero Reynolds numbers. We are capable of obtaining convergent solutions for the Reynolds number as high as 100 and the capillary number as low as 0·1.

We shall compare our numerical results with the analytical solution of Richardson,[8] the predictions of Dutta and Ryan[1] and some finite element solutions, namely the works of Omodei,[9] Ruschak[10] and Georgiou *et al.*[4]

MATHEMATICAL FORMULATION

The steady incompressible flow of a planar Newtonian jet emanating from a slot as shown in Figure 1(a) is considered. The gravitational effects are neglected in the present analysis. The equation that expresses the conservation of mass is

$$\frac{\partial \bar{u}}{\partial \bar{x}}+\frac{\partial \bar{v}}{\partial \bar{y}}=0, \tag{1}$$

and the Navier–Stokes equations in the $\bar{x}$- and $\bar{y}$-directions are

$$\rho\left(\bar{u}\frac{\partial \bar{u}}{\partial \bar{x}}+\bar{v}\frac{\partial \bar{u}}{\partial \bar{y}}\right)=-\frac{\partial \bar{p}}{\partial \bar{x}}+\mu\left(\frac{\partial^2 \bar{u}}{\partial \bar{x}^2}+\frac{\partial^2 \bar{u}}{\partial \bar{y}^2}\right), \tag{2}$$

$$\rho\left(\bar{u}\frac{\partial \bar{v}}{\partial \bar{x}}+\bar{v}\frac{\partial \bar{v}}{\partial \bar{y}}\right)=-\frac{\partial \bar{p}}{\partial \bar{y}}+\mu\left(\frac{\partial^2 \bar{v}}{\partial \bar{x}^2}+\frac{\partial^2 \bar{v}}{\partial \bar{y}^2}\right). \tag{3}$$

Owing to symmetry, we only consider the upper half of the flow regime. We assume that AS is long enough and the flow has the fully developed rectilinear velocity profile far upstream at AC, and the jet becomes unidirectional far downstream at BE. The corresponding boundary conditions are as follows.

(A1) Along AS,

$$\bar{u}=\bar{v}=0 \quad \text{(no-slip)}. \tag{4a}$$

(B1) At AC,

$$\bar{u}=-\frac{1}{2\mu}\frac{\partial \bar{p}}{\partial \bar{x}}(a^2-\bar{y}^2), \qquad \bar{v}=0. \tag{4b}$$

(C1) At BE,

$$\bar{u}=u_0, \qquad \bar{v}=0, \qquad \bar{p}=p_a, \tag{4c}$$

where p_a is the surrounding pressure.

(D1) Along CDE (line of symmetry),

$$\partial \bar{u}/\partial \bar{y}=0, \qquad \bar{v}=0. \tag{4d}$$

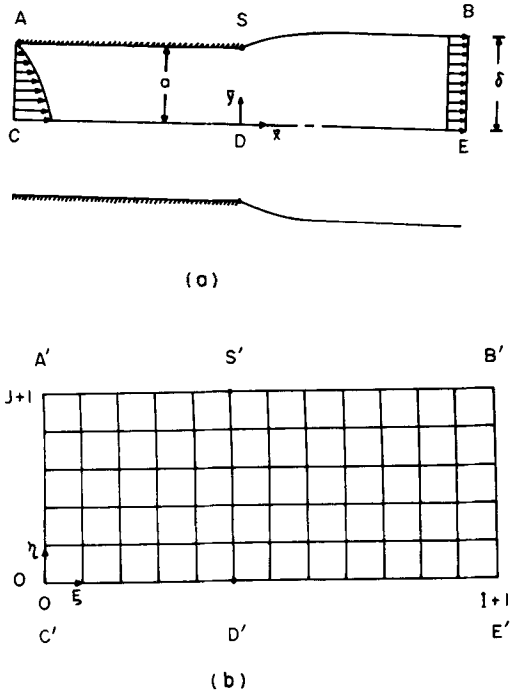

Figure 1. Flow geometry (a) in the physical plane and (b) in the transformed plane

(E1) On the free surface SB, or $\bar{y}=h(\bar{x})$, the following three conditions must be satisfied:

(i) the kinematic condition

$$\mathrm{d}h/\mathrm{d}\bar{x}=\bar{v}/\bar{u}, \tag{5a}$$

(ii) the tangential stress balance

$$\left[1-\left(\frac{\mathrm{d}h}{\mathrm{d}\bar{x}}\right)^2\right]\left(\frac{\partial\bar{u}}{\partial\bar{y}}+\frac{\partial\bar{v}}{\partial\bar{x}}\right)-2\frac{\mathrm{d}h}{\mathrm{d}\bar{x}}\left(\frac{\partial\bar{u}}{\partial\bar{x}}-\frac{\partial\bar{v}}{\partial\bar{y}}\right)=0, \tag{5b}$$

(iii) the normal stress balance

$$\left[1+\left(\frac{\mathrm{d}h}{\mathrm{d}\bar{x}}\right)^2\right]^{-1}\left[\left(\frac{\mathrm{d}h}{\mathrm{d}\bar{x}}\right)^2\left(2\mu\frac{\partial\bar{u}}{\partial\bar{x}}\right)+2\mu\frac{\partial\bar{v}}{\partial\bar{y}}-2\frac{\mathrm{d}h}{\mathrm{d}\bar{x}}\mu\left(\frac{\partial\bar{u}}{\partial\bar{y}}+\frac{\partial\bar{v}}{\partial\bar{x}}\right)\right]=\bar{p}-p_a+\bar{R}\sigma, \tag{5c}$$

where σ is the surface tension coefficient and $\bar{R}$ is the curvature of the jet surface,

$$\bar{R}\equiv\frac{\mathrm{d}^2h/\mathrm{d}\bar{x}^2}{[1+(\mathrm{d}h/\mathrm{d}\bar{x})^2]^{3/2}}. \tag{6}$$

The streamfunction $\bar{\varphi}$ and vorticity $\bar{\omega}$ are used as the dependent variables. They are defined as

$$\bar{u}\equiv\frac{\partial\bar{\varphi}}{\partial\bar{y}}, \qquad \bar{v}\equiv-\frac{\partial\bar{\varphi}}{\partial\bar{x}}, \qquad \bar{\omega}\equiv\frac{\partial\bar{v}}{\partial\bar{x}}-\frac{\partial\bar{u}}{\partial\bar{y}}. \tag{7}$$

The following dimensionless variables are defined:

$$x=\bar{x}/a, \qquad y=\bar{y}/a, \qquad H=h/a,$$
$$u=\bar{u}/\langle u\rangle, \qquad v=\bar{v}/\langle u\rangle,$$
$$p=\bar{p}/(\mu\langle u\rangle/a), \qquad \varphi=\bar{\varphi}/\langle u\rangle a, \qquad \omega=\bar{\omega}a/\langle u\rangle, \tag{8}$$

where $\langle u\rangle$ is defined as the average velocity at AC, i.e.

$$\langle u\rangle \equiv -\frac{1}{3\mu}\frac{\partial \bar{p}}{\partial \bar{x}}a^2. \tag{9}$$

Equation (1) is automatically satisfied with the definition of φ, and from (7) and (8) we have

$$\frac{\partial^2\varphi}{\partial x^2}+\frac{\partial^2\varphi}{\partial y^2}=-\omega. \tag{10}$$

Substituting the dimensionless variables into (2) and (3), we obtain

$$Re\left(u\frac{\partial u}{\partial x}+v\frac{\partial u}{\partial y}\right)=-\frac{\partial p}{\partial x}+\left(\frac{\partial^2 u}{\partial x^2}+\frac{\partial^2 u}{\partial y^2}\right), \tag{11}$$

$$Re\left(u\frac{\partial v}{\partial x}+v\frac{\partial v}{\partial y}\right)=-\frac{\partial p}{\partial y}+\left(\frac{\partial^2 v}{\partial x^2}+\frac{\partial^2 v}{\partial y^2}\right), \tag{12}$$

where the Reynolds number Re is defined as $Re=\rho\langle u\rangle a/\mu$.

The pressure terms in (11) and (12) are eliminated through cross-differentiation and we obtain the following vorticity transport equation:

$$Re\left(\frac{\partial\varphi}{\partial y}\frac{\partial\omega}{\partial x}-\frac{\partial\varphi}{\partial x}\frac{\partial\omega}{\partial y}\right)=\frac{\partial^2\omega}{\partial x^2}+\frac{\partial^2\omega}{\partial y^2}. \tag{13}$$

Equations (10) and (13) are the governing equations for the jet swell problem. Without loss of generality, we assign the line of symmetry CDE as $\varphi=0$ and the line ASB will be $\varphi=1$. The corresponding boundary conditions for (10) and (13) are as follows.

(A2) Along AS,

$$\varphi=1, \qquad \omega=\frac{\partial v}{\partial x}-\frac{\partial u}{\partial y}. \tag{14a}$$

(B2) At AC,

$$\varphi=\tfrac{1}{2}(3y-y^3), \qquad \omega=3y. \tag{14b}$$

(C2) At BE,

$$\varphi=\frac{y}{C_0}, \qquad \omega=0, \qquad p=0, \tag{14c}$$

where the jet swell ratio $C_0\equiv\delta/a$ and we take $p_a=0$ as the reference pressure.

(D2) Along CDE,

$$\varphi=0, \qquad \omega=0. \tag{14d}$$

(E2) On the free surface SB, or $y=H(x)$,

$$\varphi=1, \qquad \omega=\frac{\partial v}{\partial x}-\frac{\partial u}{\partial y}, \tag{14e}$$

and the following three conditions have to be satisfied:

(i) the kinematic condition

$$dH/dx = v/u, \tag{15a}$$

(ii) the tangential stress balance

$$\left[1-\left(\frac{dH}{dx}\right)^2\right]\left(\frac{\partial v}{\partial x}+\frac{\partial u}{\partial y}\right)-2\frac{dH}{dx}\left(\frac{\partial u}{\partial x}-\frac{\partial v}{\partial y}\right)=0, \tag{15b}$$

(iii) the normal stress balance

$$p-\frac{2}{1+(dH/dx)^2}\left[\left(\frac{dH}{dx}\right)^2\frac{\partial u}{\partial x}+\frac{\partial v}{\partial y}-\frac{dH}{dx}\left(\frac{\partial v}{\partial x}+\frac{\partial u}{\partial y}\right)\right]+\frac{R}{Ca}=0, \tag{15c}$$

where R is the dimensionless curvature and the capillary number Ca is defined as $Ca \equiv \mu\langle u\rangle/\sigma$.

It should be noted that the boundary condition for ω along ASB is expressed in terms of u and v here; this is necessary for our numerical integration and will be explained later.

CO-ORDINATE TRANSFORMATION

Since the free surface of the jet may have different shapes, it is awkward to solve the jet swell problem with conventional finite difference methods. Dutta and Ryan[1] selected an orthogonal transformation method to map the flow region into a rectangular domain to avoid a direct fitting of the jet surface with the grid points. We adopted a more flexible technique, the boundary-fitted co-ordinate transformation method developed by Thompson *et al.*,[6,7] for our numerical mapping. The upper half of the flow regime in Figure 1(a) will be transformed into a rectangular domain with (ξ, η) as independent variables. The correspondence between the (x, y) and the (ξ, η) plane is shown in Figure 1(b). To apply the method of Thompson *et al.*, we need to solve the following mapping equations:

$$\alpha\frac{\partial^2 x}{\partial \xi^2}-2\beta\frac{\partial^2 x}{\partial \xi \partial \eta}+\gamma\frac{\partial^2 x}{\partial \eta^2}=-\lambda^2\left(M(\xi,\eta)\frac{\partial x}{\partial \xi}+N(\xi,\eta)\frac{\partial x}{\partial \eta}\right), \tag{16a}$$

$$\alpha\frac{\partial^2 y}{\partial \xi^2}-2\beta\frac{\partial^2 y}{\partial \xi \partial \eta}+\gamma\frac{\partial^2 y}{\partial \eta^2}=-\lambda^2\left(M(\xi,\eta)\frac{\partial y}{\partial \xi}+N(\xi,\eta)\frac{\partial y}{\partial \eta}\right), \tag{16b}$$

where

$$\begin{aligned} \alpha &= \left(\frac{\partial x}{\partial \eta}\right)^2+\left(\frac{\partial y}{\partial \eta}\right)^2, & \beta &= \frac{\partial x}{\partial \xi}\frac{\partial x}{\partial \eta}+\frac{\partial y}{\partial \xi}\frac{\partial y}{\partial \eta}, \\ \gamma &= \left(\frac{\partial x}{\partial \xi}\right)^2+\left(\frac{\partial y}{\partial \xi}\right)^2, & \lambda &= \frac{\partial x}{\partial \xi}\frac{\partial y}{\partial \eta}-\frac{\partial y}{\partial \xi}\frac{\partial x}{\partial \eta}, \end{aligned} \tag{16c}$$

λ is the Jacobian of the transformation and $M(\xi, \eta)$ and $N(\xi, \eta)$ are forcing functions that are used to regulate mesh intervals.

To solve (16), Dirichlet boundary conditions are imposed on the boundary of the rectangular domain in Figure 1(b). Since each grid point on the boundary of the rectangle should be assigned to a boundary point in the physical domain in Figure 1(a), the co-ordinates (x, y) of the boundary

point become the required boundary values of this grid point. A detailed description of this procedure is explained in the next section.

Equations (10) and (13) should be transformed to the (ξ, η) plane accordingly, and we have

$$\alpha\frac{\partial^2\varphi}{\partial\xi^2}-2\beta\frac{\partial^2\varphi}{\partial\xi\partial\eta}+\gamma\frac{\partial^2\varphi}{\partial\eta^2}=-\lambda^2\left(M\frac{\partial\varphi}{\partial\xi}+N\frac{\partial\varphi}{\partial\eta}+\omega\right), \tag{17}$$

$$\alpha\frac{\partial^2\omega}{\partial\xi^2}-2\beta\frac{\partial^2\omega}{\partial\xi\partial\eta}+\gamma\frac{\partial^2\omega}{\partial\eta^2}=\lambda^2\left[\left(\frac{Re}{\lambda}\frac{\partial\varphi}{\partial\eta}-M\right)\frac{\partial\omega}{\partial\xi}-\left(\frac{Re}{\lambda}\frac{\partial\varphi}{\partial\xi}+N\right)\frac{\partial\omega}{\partial\eta}\right]. \tag{18}$$

To simplify our numerical procedure, the forcing functions M and N are taken to be zero in our work this corresponds to the harmonic mapping discussed by Thompson *et al.*[7] u, v and ω can be expressed as follows:

$$u=\frac{\partial\varphi}{\partial y}=-\frac{1}{\lambda}\left(\frac{\partial\varphi}{\partial\xi}\frac{\partial x}{\partial\eta}-\frac{\partial\varphi}{\partial\eta}\frac{\partial x}{\partial\xi}\right), \tag{19a}$$

$$v=-\frac{\partial\varphi}{\partial x}=-\frac{1}{\lambda}\left(\frac{\partial\varphi}{\partial\xi}\frac{\partial y}{\partial\eta}-\frac{\partial\varphi}{\partial\eta}\frac{\partial y}{\partial\xi}\right), \tag{19b}$$

$$\omega=\frac{\partial v}{\partial x}-\frac{\partial u}{\partial y}=\frac{1}{\lambda}\left(\frac{\partial v}{\partial\xi}\frac{\partial y}{\partial\eta}-\frac{\partial v}{\partial\eta}\frac{\partial y}{\partial\xi}+\frac{\partial u}{\partial\xi}\frac{\partial x}{\partial\eta}-\frac{\partial u}{\partial\eta}\frac{\partial x}{\partial\xi}\right). \tag{19c}$$

To determine the pressure, we first transform (11) and (12) to the (ξ, η) plane:

$$Re\left[u\left(\frac{\partial u}{\partial\xi}\frac{\partial y}{\partial\eta}-\frac{\partial u}{\partial\eta}\frac{\partial y}{\partial\xi}\right)-v\left(\frac{\partial u}{\partial\xi}\frac{\partial x}{\partial\eta}-\frac{\partial u}{\partial\eta}\frac{\partial x}{\partial\xi}\right)\right]=-\left(\frac{\partial p}{\partial\xi}\frac{\partial y}{\partial\eta}-\frac{\partial p}{\partial\eta}\frac{\partial y}{\partial\xi}\right)+\left(\frac{\partial\omega}{\partial\xi}\frac{\partial x}{\partial\eta}-\frac{\partial\omega}{\partial\eta}\frac{\partial x}{\partial\xi}\right), \tag{20}$$

$$Re\left[u\left(\frac{\partial v}{\partial\xi}\frac{\partial y}{\partial\eta}-\frac{\partial v}{\partial\eta}\frac{\partial y}{\partial\xi}\right)-v\left(\frac{\partial v}{\partial\xi}\frac{\partial x}{\partial\eta}-\frac{\partial v}{\partial\eta}\frac{\partial x}{\partial\xi}\right)\right]=+\left(\frac{\partial p}{\partial\xi}\frac{\partial x}{\partial\eta}-\frac{\partial p}{\partial\eta}\frac{\partial x}{\partial\xi}\right)+\left(\frac{\partial\omega}{\partial\xi}\frac{\partial y}{\partial\eta}-\frac{\partial\omega}{\partial\eta}\frac{\partial y}{\partial\xi}\right); \tag{21}$$

note here that ω is introduced into the right-hand side of the equations to replace u and v.

The term $\partial p/\partial\eta$ can be eliminated in these two equations; we obtain

$$\begin{aligned}-\frac{\partial p}{\partial\xi}=\frac{1}{\lambda}\left(\gamma\frac{\partial\omega}{\partial\eta}-\beta\frac{\partial\omega}{\partial\xi}\right)+\frac{Re}{\lambda}\Bigg\{u\Bigg[\left(\frac{\partial u}{\partial\xi}\frac{\partial y}{\partial\eta}-\frac{\partial u}{\partial\eta}\frac{\partial y}{\partial\xi}\right)\frac{\partial x}{\partial\xi}+\left(\frac{\partial v}{\partial\xi}\frac{\partial y}{\partial\eta}-\frac{\partial v}{\partial\eta}\frac{\partial y}{\partial\xi}\right)\frac{\partial y}{\partial\xi}\Bigg]\\ -v\Bigg[\left(\frac{\partial u}{\partial\xi}\frac{\partial x}{\partial\eta}-\frac{\partial u}{\partial\eta}\frac{\partial x}{\partial\xi}\right)\frac{\partial x}{\partial\xi}+\left(\frac{\partial v}{\partial\xi}\frac{\partial x}{\partial\eta}-\frac{\partial v}{\partial\eta}\frac{\partial x}{\partial\xi}\right)\frac{\partial y}{\partial\xi}\Bigg]\Bigg\}.\end{aligned} \tag{22}$$

Equation (22) is used to approximate the pressure distribution in our computation.

The corresponding boundary conditions in the transformed plane are as follows.

(A3) Along A′S′,

$$\varphi=1, \qquad \omega=\frac{1}{\lambda}\left(\frac{\partial v}{\partial\xi}\frac{\partial y}{\partial\eta}-\frac{\partial v}{\partial\eta}\frac{\partial y}{\partial\xi}+\frac{\partial u}{\partial\xi}\frac{\partial x}{\partial\eta}-\frac{\partial u}{\partial\eta}\frac{\partial x}{\partial\xi}\right). \tag{23}$$

(B3) At A′C′,

$$\varphi=\tfrac{1}{2}(3y-y^3), \qquad \omega=3y. \tag{24}$$

(C3) At B′F′,

$$\varphi=y/C_0, \qquad \omega=0, \qquad p=0. \tag{25}$$

(D3) Along C'E',

$$\varphi = 0, \qquad \omega = 0. \tag{26}$$

(E3) On the free surface S'B',

$$\varphi = 1, \qquad \omega = \frac{1}{\lambda}\left(\frac{\partial v}{\partial \xi}\frac{\partial y}{\partial \eta} - \frac{\partial v}{\partial \eta}\frac{\partial y}{\partial \xi} + \frac{\partial u}{\partial \xi}\frac{\partial x}{\partial \eta} - \frac{\partial u}{\partial \eta}\frac{\partial x}{\partial \xi}\right), \tag{27}$$

and the following three conditions have to be satisfied:

(i) the kinematic condition

$$\frac{\mathrm{d}H}{\mathrm{d}x} = \frac{v}{u} = \frac{\partial y/\partial \xi}{\partial x/\partial \xi}, \tag{28}$$

(ii) the tangential stress balance

$$\frac{\partial u}{\partial \eta} = \frac{1}{\gamma}\left(\beta\frac{\partial y/\partial \xi}{\partial x/\partial \xi} - \lambda\right)\frac{\partial v}{\partial \xi} - \frac{\partial y/\partial \xi}{\partial x/\partial \xi}\frac{\partial v}{\partial \eta} + \frac{1}{\gamma}\left(\beta + \lambda\frac{\partial y/\partial \xi}{\partial x/\partial \xi}\right)\frac{\partial u}{\partial \xi}, \tag{29}$$

(iii) the normal stress balance

$$\frac{\partial v}{\partial \eta} = \frac{\beta}{\gamma}\frac{\partial v}{\partial \xi} - \frac{\beta}{\gamma}\frac{\partial y/\partial \xi}{\partial x/\partial \xi}\frac{\partial u}{\partial \xi} + \frac{\partial y/\partial \xi}{\partial x/\partial \xi}\frac{\partial u}{\partial \eta} + \frac{\lambda}{2\partial x/\partial \xi}\left(p + \frac{R}{Ca}\right). \tag{30}$$

NUMERICAL PROCEDURE

The mapping equations (16) and equations (17)–(30) that describe the fluid motion in the transformed plane will be solved numerically by the finite difference method. We use second-order formulae to discretize these equations. The rectangular domain in Figure 1(b) is divided into $I+1$ segments in the ξ-direction and $J+1$ segments in the η-direction. Hence $i=0, I+1$ correspond to the boundary lines in the ξ-direction, and $j=0, J+1$ correspond to the boundary lines in the η-direction.

For a function $f(\xi, \eta)$, its first and second derivatives can be approximated as[11]

$$\begin{aligned}
(f_\xi)_{i,j} &= (1/2r)\,(f_{i+1,j} - f_{i-1,j}),\\
(f_\eta)_{i,j} &= (1/2s)\,(f_{i,j+1} - f_{i,j-1}),\\
(f_{\xi\xi})_{i,j} &= (1/r^2)\,(f_{i+1,j} - 2f_{i,j} + f_{i-1,j}),\\
(f_{\eta\eta})_{i,j} &= (1/s^2)\,(f_{i,j+1} - 2f_{i,j} + f_{i,j-1}),\\
(f_{\xi\eta})_{i,j} &= (1/4rs)\,(f_{i+1,j+1} - f_{i+1,j-1} - f_{i-1,j+1} + f_{i-1,j-1}),
\end{aligned} \tag{31}$$

where subscripts denote partial differentiation, $r \equiv \Delta\xi$, $s \equiv \Delta\eta$, $\xi_i \equiv ir$, $\eta_j \equiv js$ and $f_{i,j}$ stands for $f(\xi_i, \eta_j)$.

Derivatives on the boundary can be approximated using one-sided formulae:[12]

$$\begin{aligned}
(f_\xi)_{0,j} &= (1/2r)\,(-f_{2,j} + 4f_{1,j} - 3f_{0,j}),\\
(f_\eta)_{i,0} &= (1/2s)\,(-f_{i,2} + 4f_{i,1} - 3f_{i,0}),\\
(f_\xi)_{I+1,j} &= (1/2r)\,(f_{I-1,j} - 4f_{I,j} + 3f_{I+1,j}),\\
(f_\eta)_{i,J+1} &= (1/2s)\,(f_{i,J-1} - 4f_{i,J} + 3f_{i,J+1}).
\end{aligned} \tag{32}$$

The numerical procedure for solving the jet flow problem consists of three steps, as follows.

(I) Numerical mapping

The mapping procedure follows the work of Thompson *et al.*[6,7] The upstream length CD and downstream length DE are selected on the basis of Tanner's criterion[2] so that the appropriate boundary conditions can be applied at AC and BE. The position of the free surface SB should be guessed and the initial flow regime for the numerical integration is completely determined. After non-dimensionalization, the boundary of the flow regime is discretized and the corresponding mesh points on the boundary of the rectangle in Figure 1(a) should be assigned first; the guessed values of the interior mesh points (x, y) in the (ξ, η) plane should be given. The coefficients α, β, γ and λ in (16c) are estimated with guessed values of x and y using (31). After discretizing (16a) and (16b) with (31), the resulting linear systems of equations are solved by the successive line overrelaxation method. The newly generated values of (x, y) are compared with the guessed values as a convergence test. The iterative process will continue until convergence is achieved. Values of α, β, γ and λ will be used later in the flow equations.

(II) Solution of the flow equations

The procedure for solving the flow equations is given as follows.

1. Guess φ and ω, say φ^0 and ω^0, on all interior grid points in the (ξ, η) plane. C_0 in (25) should also be guessed.
2. Using (19a) and (19b), u^0 and v^0 on A′S′B′ can be estimated with guessed values of φ^0 on A′S′B′ and on two grid lines below; then ω^0 on A′S′B′ can be computed using (19c). This will determine the boundary condition for ω on A′S′B′.
3. Equations (17) and (18) are solved by the successive line underrelaxation method to generate new values of φ and ω, say φ^1 and ω^1, for all interior grid points. Note that the terms on the right-hand side of (17) and (18) are approximated with values of φ^0 and ω^0 during the iteration.
4. Values of ω, say ω^1, on the wall A′S′ are updated with the same method as step 2, i.e. u^1 and v^1 are first determined and then ω^1 is determined with (19).
5. The pressure p at B′E′ is assumed to be zero and the value of p at each grid point to the left of B′E′ can be computed using (22). However, during the iteration process, only values of p on the free surface S′B′ are needed.
6. Equation (29) is used to update u on the free surface S′B′. All the terms on the right-hand side of the equation are approximated using u^1 and v^1 obtained in step 4. The term $\partial u/\partial \eta$ is discretized with (32) to update u on S′B′. A new value of u, say $u^{(1+1/2)}$, is generated at each grid point on S′B′. Similarly, (30) is used to update v on S′B′ and we can obtain $v^{(1+1/2)}$. The pressure on the free surface in step 5 is needed in (30).
7. ω on the free surface S′B′ is updated using (19c) with $u^{(1+1/2)}$ and $v^{(1+1/2)}$, and we will have ω^1.
8. Check convergence. φ^1 and ω^1 will be compared with φ^0 and ω^0 for all interior points and ω^1 will be compared with ω^0 on A′S′B′.

If the maximum difference between guessed values and newly generated values is smaller than a preset tolerance, we can update u, v and p, then go to (III), otherwise we will replace φ^0 by φ^1 and ω^0 by ω^1 and return to step 3.

(III) Updating the free surface

With the convergent solution of u and v on the free surface available, we can use (28) to generate a new position of the free surface. Equation (28) can be integrated numerically starting from the

separation point as follows:

$$H(x)=\int_0^x \frac{v}{u}\,\mathrm{d}x. \tag{33}$$

We use the trapezoidal rule to obtain $H(x)$ on the first grid point downstream, then the remaining points are computed using Simpson's rule. Once a new position of the free surface is generated, we continue the convergence check by comparing it with the current position of the free surface on each grid point in the physical plane. If convergence is achieved, i.e. the maximum difference of the two free surface positions is smaller than a preset value, our computation is complete; otherwise the current free-surface position is updated and the iteration is repeated starting from (I). We have found that if we replace the current free-surface position by the new free-surface position determined by (33), we cannot obtain convergent solutions for the case of high Re. Therefore it is necessary to update the free-surface position as follows:

$$H(x)^{\mathrm{new}} = (1-k)\,H(x)^{1} + kH(x)^{\mathrm{old}}, \tag{34}$$

where $H(x)^{\mathrm{new}}$ is the new free-surface position for the next iteration, $H(x)^{1}$ is determined by (33), $H(x)^{\mathrm{old}}$ is the current free-surface position and k is an adjustable parameter, which varies between 0 and 0·98 in our computation. As Re increases, it is necessary to increase k to obtain convergent solutions. The jet swell ratio C_0 is the dimensionless jet thickness far downstream, i.e. C_0 is equal to $H(x)$ at B′E′.

RESULTS AND DISCUSSION

All of our computations were performed on a CDC Cyber 180/840 machine. The tolerance of convergence was fixed to be $1{\cdot}0 \times 10^{-4}$ for all tests.

The swelling of a creeping Newtonian jet with $Ca = 1000$ was first selected as a test case. We took $\Delta x = \Delta y$ for convenience in our computation and the step size was systematically reduced from 0·5 to 0·05. It was found that the difference in the swell ratio for the cases $\Delta x = 0{\cdot}1$ and $\Delta x = 0{\cdot}05$ was less than 0·1%. We also tested the case with $Re = 100$ and $Ca = 1000$ and found that the numerical results for $\Delta x = 0{\cdot}1$ and $\Delta x = 0{\cdot}05$ were almost identical. Therefore $\Delta x = \Delta y = 0{\cdot}1$ was fixed for all the following runs.

We also used the problem of the creeping Newtonian jet to experimentally determine the optimal relaxation factor. The optimal relaxation factor for mapping was tested between 0·3 and 1·7; it was found that the value 1·5 would need the least computing time, and 1·5 was therefore chosen as the optimal overrelaxation factor. Similarly, the underrelaxation factor for solving the flow equations was tested between 0·2 and 0·9, and 0·9 appeared to be the optimal underrelaxation factor. These two factors were also fixed for the following runs.

To illustrate the CPU time required, a standard mesh with $\Delta x = \Delta y = 0{\cdot}1$ was set up for the creeping Newtonian jet problem. The upstream length was selected to be 2 and downstream length was 13. There were a total of 151 × 11 mesh points. The initial profile for the free surface was selected as

$$y=\delta_0+(1-\delta_0)\mathrm{e}^{-\bar{A}x}, \tag{35}$$

where $\delta_0 = 0{\cdot}95$ and $\bar{A} = 6{\cdot}5$. It took 113·2 CPU seconds to generate the convergent solution, and the location of the free surface, which can be computed by (III) in the previous section, was updated 24 times. A portion of the numerically simulated jet near the separation point is shown in Figure 2; note that only grid lines with $\Delta x = \Delta y = 0{\cdot}2$ are given in the figure.

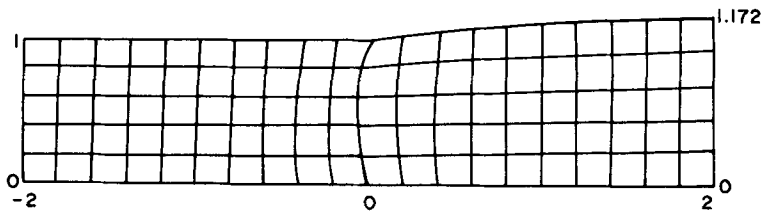

Figure 2. The shape and mesh of a creeping Newtonian jet with $Ca = 1000$

Table I. Values of k with $Ca = 1000$

Re	k
0	0·00
10	0·10
20	0·70
40	0·80
60	0·90
80	0·93
100	0·98

The convergent solution for the creeping Newtonian jet was used as the initial guess to produce numerical solutions for high Re. Usually, Re was incremented by 10 and a series of solutions could be generated. The numerical scheme was not sensitive to the variation of Ca. Initially, k was selected to be zero; if the iteration failed to converge after the free surface was updated a certain number of times, k would be reduced. We found that the iteration would either diverge or converge before the free surface was updated 20 times. Suitable values of k that lead to fast convergence for different Reynolds numbers are given in Table I. With this approach we could obtain convergent solutions for Re as high as 100 and Ca as low as 0·1.

The adjustable parameter k we used in the free-surface iteration is similar to the 'damping factor' introduced by Omodei.[9] We found that k depends strongly on the Reynolds number whereas the damping factor of Omodei depends only on the capillary number. Actually, the capillary number did not appear in Omodei's formulation explicitly; a surface tension parameter $\bar{S}$ was defined such that $Ca = Re/\bar{S}$, $\bar{S}$ and Re were varied separately to test convergence. In our computation, only Re appears in the iteration process (step 3 in (II)), whereas Ca is needed in updating v on the free surface (step 6 in (II)); therefore Re was found to be the only critical parameter for convergence.

We also tested the effects of upstream and downstream length on the numerical solution. It should be noted that Omodei[9] and Georgiou *et al.*[4] used the primitive variables u, v and p as dependent variables in their finite element simulation, and the downstream length has to be longer than 75 to generate accurate numerical solutions for the case of high Re. Our finite difference simulation is based on the streamfunction–vorticity formulation; we tested the upstream length from $x = -2$ to -4 and found that $x = -3$ was satisfactory for the range of Re we studied. The downstream length was checked from $x = 12$ to 20 and it was found that the numerical results were almost identical for $x = 13$ and 20 with $Re = 100$.

We first compared our numerical results with Richardson's exact solution[8] in terms of pressure variation. The pressure along the centreline of the flow system is shown in Figure 3. Inside the slot

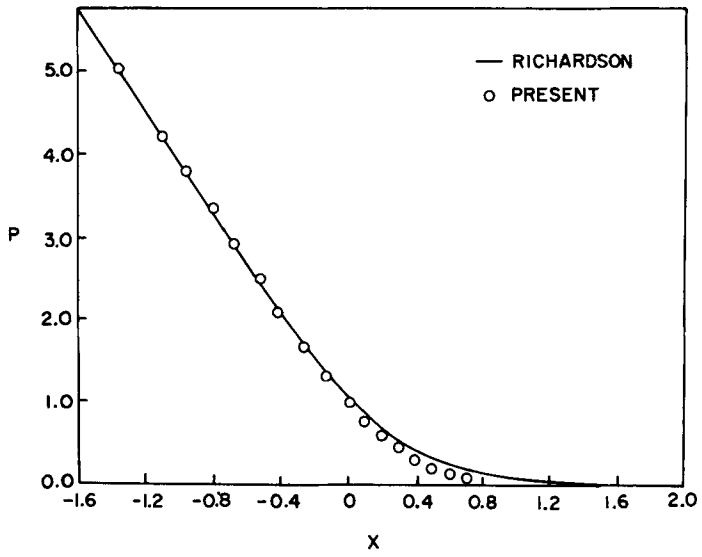

Figure 3. Comparison of pressure distribution along the centreline of the flow system with Richardson's solution[9]

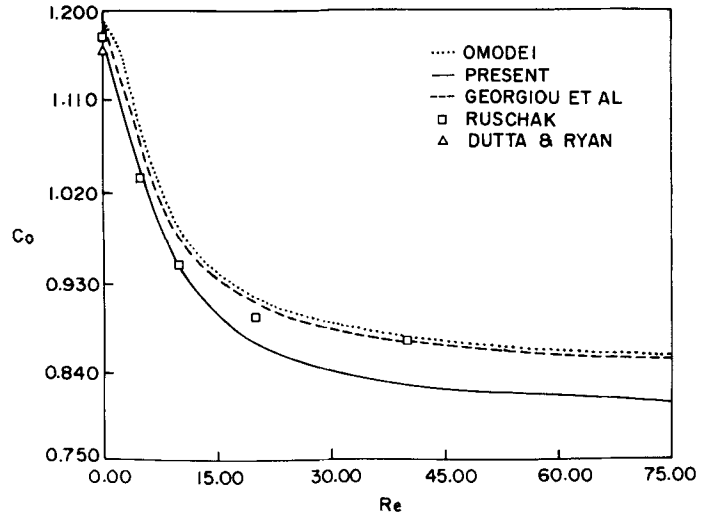

Figure 4. Comparison of the jet swell ratio with previous works

the agreement is excellent; the pressure we computed in the jet is slightly lower than Richardson's prediction.

A comparison of the jet swell ratio with previous works[1,4,9,10] is given in Figure 4. Values of the jet swell ratio C_0 computed by the BFCTM are close to those of finite element simulations if the Reynolds number is low. However, as Re increases, C_0 predicted by the BFCTM is about 5% lower than previous works that were based on the finite element method.

The shapes of the creeping Newtonian jet determined by different numerical approaches are given in Figure 5. All the authors found that the jet will reach its final thickness at a downstream

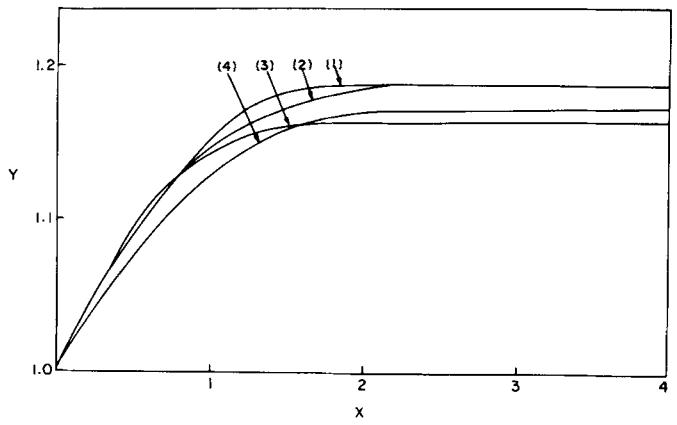

Figure 5. Comparison of the surface shapes for a creeping Newtonian jet with $Ca = 1000$: (1) Ruschak;[10] (2) Omodei;[9] (3) Dutta and Ryan;[1] (4) present

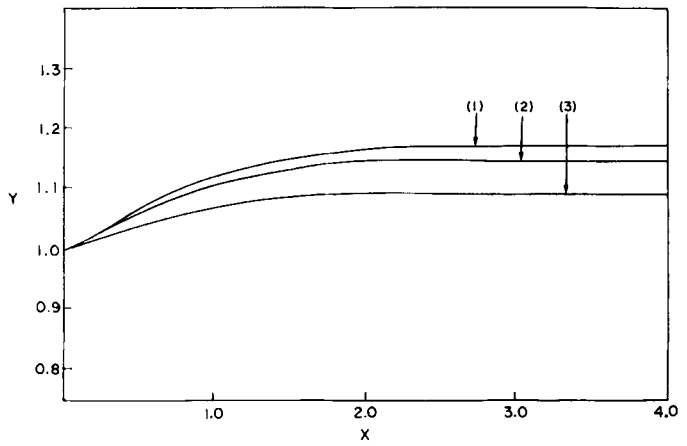

Figure 6. Effect of Ca on the jet free surface with $Re = 1$: (1) $Ca = 1000$; (2) $Ca = 2{\cdot}0$; (3) $Ca = 0{\cdot}5$

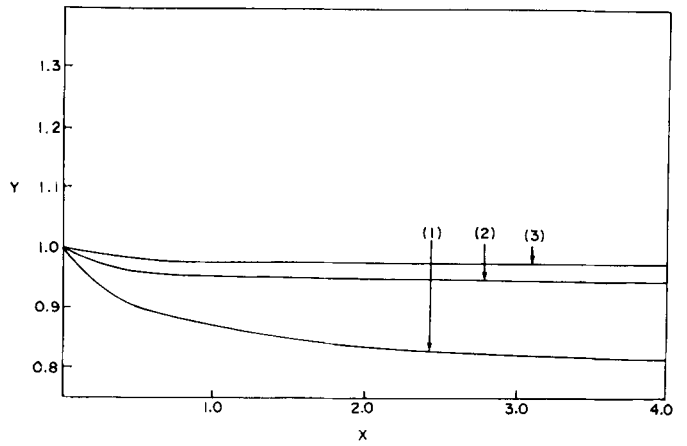

Figure 7. Effects of Ca and Re on the jet free surface: (1) $Re = 100$, $Ca = 1000$; (2) $Re = 10$, $Ca = 1000$; (3) $Re = 10$, $Ca = 0{\cdot}5$

Table II. A comparison of errors on the jet surface with $Re = 0$, $Ca = 1000$

Omodei[9]			Dutta and Ryan[1]				Present			
x	Tn	Ts	x	Tn	Ts	$\bar{D}$	x	Tn	Ts	$\bar{D}$
0·06	-0.0389	-0.1390	0·0676	0.026×10^{-3}	1.827×10^{-3}	5·141	0·10	0.430×10^{-3}	0.728×10^{-1}	1.3126
0·30	-0.0351	-0.0054	0·1557	1.453×10^{-3}	0.990×10^{-3}	2·853	0·20	0.384×10^{-3}	-0.323×10^{-1}	-0.5539
0·40	-0.0070	-0.0067	0·2537	1.935×10^{-3}	0.700×10^{-3}	2·471	0·30	0.355×10^{-4}	-0.454×10^{-2}	-0.1428
0·50	-0.0184	-0.0070	0·5729	1.635×10^{-3}	0.101×10^{-3}	1·481	0·40	0.584×10^{-4}	-0.178×10^{-2}	-0.1092
0·80	-0.0088	-0.0043	1·0200	0.652×10^{-3}	-0.275×10^{-3}	0·611	0·50	0.633×10^{-4}	-0.643×10^{-3}	-0.0647
1·30	-0.0031	0·0013	1·5810	0.050×10^{-3}	-0.238×10^{-3}	0·107	0·60	0.327×10^{-4}	-0.300×10^{-3}	-0.0425
2·00	-0.0002	0·0016					0·70	0.295×10^{-6}	-0.136×10^{-3}	-0.0289
3·50	-0.0002	0·0008					0·80	-0.107×10^{-4}	-0.767×10^{-4}	-0.0203
7·00	3.0×10^{-6}	2.0×10^{-5}					0·90	-0.765×10^{-5}	-0.707×10^{-4}	-0.0147
9·50	-3.0×10^{-6}	-3.0×10^{-6}					1·00	-0.277×10^{-5}	-0.695×10^{-4}	-0.0107
							1·30	0.205×10^{-5}	-0.439×10^{-4}	-0.0042
							1·60	-0.832×10^{-7}	0.141×10^{-4}	-0.0014
							2·00	-0.198×10^{-6}	-0.751×10^{-5}	-0.5×10^{-4}
							3.50	-0.826×10^{-8}	-0.448×10^{-5}	-0.2×10^{-4}
							7·00	0.79×10^{-9}	-0.856×10^{-6}	-0.6×10^{-5}
							9·50	-0.737×10^{-8}	-0.108×10^{-4}	-0.6×10^{-5}

Table III. The effect of Re on free-surface errors

	$Re = 1, \quad Ca = 1000$			$Re = 100, \quad Ca = 1000$		
x	Ts	Tn	$\bar{D}$	Ts	Tn	$\bar{D}$
$0{\cdot}10 \times 10^{0}$	$0{\cdot}86639 \times 10^{-1}$	$0{\cdot}71252 \times 10^{-3}$	$0{\cdot}11949 \times 10^{1}$	$0{\cdot}87608 \times 10^{-1}$	$0{\cdot}15928 \times 10^{-1}$	$0{\cdot}52369 \times 10^{0}$
$0{\cdot}20 \times 10^{0}$	$-0{\cdot}31798 \times 10^{-1}$	$0{\cdot}48400 \times 10^{-3}$	$-0{\cdot}51581 \times 10^{0}$	$-0{\cdot}80049 \times 10^{-1}$	$0{\cdot}17301 \times 10^{-1}$	$-0{\cdot}16288 \times 10^{0}$
$0{\cdot}30 \times 10^{0}$	$-0{\cdot}46033 \times 10^{-2}$	$0{\cdot}17670 \times 10^{-3}$	$-0{\cdot}13953 \times 10^{0}$	$-0{\cdot}66037 \times 10^{-1}$	$-0{\cdot}27256 \times 10^{-2}$	$-0{\cdot}83168 \times 10^{-1}$
$0{\cdot}40 \times 10^{0}$	$-0{\cdot}18016 \times 10^{-2}$	$0{\cdot}73855 \times 10^{-4}$	$-0{\cdot}10290 \times 10^{0}$	$-0{\cdot}44365 \times 10^{-1}$	$-0{\cdot}13072 \times 10^{-1}$	$-0{\cdot}10381 \times 10^{0}$
$0{\cdot}50 \times 10^{0}$	$-0{\cdot}59783 \times 10^{-3}$	$0{\cdot}52456 \times 10^{-5}$	$-0{\cdot}61490 \times 10^{-1}$	$-0{\cdot}20241 \times 10^{-1}$	$-0{\cdot}14163 \times 10^{-1}$	$-0{\cdot}92972 \times 10^{0}$
$0{\cdot}60 \times 10^{0}$	$-0{\cdot}26987 \times 10^{-3}$	$-0{\cdot}23611 \times 10^{-4}$	$-0{\cdot}40734 \times 10^{-1}$	$0{\cdot}80580 \times 10^{-2}$	$-0{\cdot}87266 \times 10^{-2}$	$-0{\cdot}52058 \times 10^{-1}$
$0{\cdot}70 \times 10^{0}$	$-0{\cdot}18725 \times 10^{-3}$	$-0{\cdot}15324 \times 10^{-4}$	$-0{\cdot}28037 \times 10^{-1}$	$0{\cdot}34732 \times 10^{-1}$	$-0{\cdot}38619 \times 10^{-3}$	$0{\cdot}13673 \times 10^{-1}$
$0{\cdot}80 \times 10^{0}$	$-0{\cdot}13925 \times 10^{-3}$	$-0{\cdot}15209 \times 10^{-4}$	$-0{\cdot}19992 \times 10^{-1}$	$0{\cdot}50232 \times 10^{-1}$	$0{\cdot}70756 \times 10^{-2}$	$0{\cdot}85870 \times 10^{-1}$
$0{\cdot}90 \times 10^{0}$	$-0{\cdot}12450 \times 10^{-3}$	$-0{\cdot}63698 \times 10^{-5}$	$-0{\cdot}14560 \times 10^{-1}$	$0{\cdot}45522 \times 10^{-1}$	$0{\cdot}10989 \times 10^{-1}$	$0{\cdot}13815 \times 10^{0}$
$0{\cdot}10 \times 10^{1}$	$-0{\cdot}14196 \times 10^{-3}$	$0{\cdot}67965 \times 10^{-5}$	$-0{\cdot}10683 \times 10^{-1}$	$0{\cdot}20576 \times 10^{-1}$	$0{\cdot}10597 \times 10^{-1}$	$0{\cdot}15148 \times 10^{0}$
$0{\cdot}20 \times 10^{1}$	$-0{\cdot}32201 \times 10^{-4}$	$0{\cdot}11340 \times 10^{-5}$	$0{\cdot}86063 \times 10^{-3}$	$0{\cdot}12366 \times 10^{-1}$	$0{\cdot}21806 \times 10^{-4}$	$0{\cdot}69004 \times 10^{-1}$
$0{\cdot}30 \times 10^{1}$	$0{\cdot}30081 \times 10^{-5}$	$-0{\cdot}36075 \times 10^{-7}$	$0{\cdot}50065 \times 10^{-3}$	$-0{\cdot}30023 \times 10^{-2}$	$0{\cdot}11228 \times 10^{-3}$	$0{\cdot}26745 \times 10^{-2}$
$0{\cdot}40 \times 10^{1}$	$-0{\cdot}37976 \times 10^{-5}$	$-0{\cdot}69723 \times 10^{-8}$	$-0{\cdot}11788 \times 10^{-3}$	$0{\cdot}27071 \times 10^{-2}$	$-0{\cdot}59719 \times 10^{-4}$	$-0{\cdot}14701 \times 10^{0}$
$0{\cdot}50 \times 10^{1}$	$0{\cdot}30423 \times 10^{-6}$	$0{\cdot}35319 \times 10^{-9}$	$-0{\cdot}11986 \times 10^{-3}$	$-0{\cdot}48996 \times 10^{-2}$	$0{\cdot}83790 \times 10^{-4}$	$-0{\cdot}97360 \times 10^{-1}$
$0{\cdot}60 \times 10^{1}$	$-0{\cdot}68685 \times 10^{-5}$	$0{\cdot}51123 \times 10^{-9}$	$-0{\cdot}59879 \times 10^{-4}$	$0{\cdot}10876 \times 10^{-1}$	$0{\cdot}22971 \times 10^{-3}$	$-0{\cdot}26158 \times 10^{0}$
$0{\cdot}70 \times 10^{1}$	$-0{\cdot}22370 \times 10^{-5}$	$0{\cdot}60012 \times 10^{-9}$	$-0{\cdot}30153 \times 10^{-4}$	$-0{\cdot}78991 \times 10^{-2}$	$-0{\cdot}20124 \times 10^{-3}$	$-0{\cdot}19677 \times 10^{0}$
$0{\cdot}80 \times 10^{1}$	$0{\cdot}14650 \times 10^{-4}$	$-0{\cdot}95105 \times 10^{-9}$	$-0{\cdot}27289 \times 10^{-4}$	$0{\cdot}16541 \times 10^{-1}$	$-0{\cdot}40949 \times 10^{-4}$	$0{\cdot}74107 \times 10^{-1}$
$0{\cdot}90 \times 10^{1}$	$-0{\cdot}44338 \times 10^{-5}$	$-0{\cdot}50500 \times 10^{-9}$	$-0{\cdot}70176 \times 10^{-5}$	$-0{\cdot}29519 \times 10^{-1}$	$-0{\cdot}30972 \times 10^{-3}$	$-0{\cdot}16318 \times 10^{-3}$
$0{\cdot}10 \times 10^{2}$	$-0{\cdot}38431 \times 10^{-5}$	$-0{\cdot}12886 \times 10^{-7}$	$-0{\cdot}17772 \times 10^{-4}$	$0{\cdot}15319 \times 10^{-1}$	$0{\cdot}96512 \times 10^{-4}$	$0{\cdot}22798 \times 10^{-1}$

Table IV. The effect of Ca on free-surface errors

	$Re = 10, \quad Ca = 0{\cdot}5$			$Re = 10, \quad Ca = 1000$		
x	Ts	Tn	$\bar{D}$	Ts	Tn	$\bar{D}$
$0{\cdot}10 \times 10^{0}$	$0{\cdot}92495 \times 10^{-1}$	$0{\cdot}11216 \times 10^{-2}$	$0{\cdot}78192 \times 10^{0}$	$0{\cdot}13070 \times 10^{0}$	$0{\cdot}21855 \times 10^{-2}$	$0{\cdot}69979 \times 10^{0}$
$0{\cdot}20 \times 10^{0}$	$-0{\cdot}55930 \times 10^{-1}$	$0{\cdot}91221 \times 10^{-3}$	$-0{\cdot}24919 \times 10^{0}$	$-0{\cdot}31125 \times 10^{-1}$	$0{\cdot}25341 \times 10^{-3}$	$-0{\cdot}29799 \times 10^{0}$
$0{\cdot}30 \times 10^{0}$	$0{\cdot}12952 \times 10^{-1}$	$0{\cdot}56130 \times 10^{-4}$	$-0{\cdot}18977 \times 10^{0}$	$-0{\cdot}59163 \times 10^{-2}$	$0{\cdot}14008 \times 10^{-4}$	$-0{\cdot}11152 \times 10^{0}$
$0{\cdot}40 \times 10^{0}$	$-0{\cdot}12625 \times 10^{-1}$	$0{\cdot}70688 \times 10^{-4}$	$-0{\cdot}48838 \times 10^{-1}$	$-0{\cdot}29240 \times 10^{-2}$	$0{\cdot}44465 \times 10^{-5}$	$-0{\cdot}72503 \times 10^{-1}$
$0{\cdot}50 \times 10^{0}$	$-0{\cdot}14843 \times 10^{-2}$	$0{\cdot}13271 \times 10^{-5}$	$-0{\cdot}46987 \times 10^{-1}$	$-0{\cdot}21013 \times 10^{-2}$	$0{\cdot}17945 \times 10^{-5}$	$-0{\cdot}43248 \times 10^{-1}$
$0{\cdot}60 \times 10^{0}$	$-0{\cdot}28747 \times 10^{-2}$	$0{\cdot}42840 \times 10^{-5}$	$-0{\cdot}23771 \times 10^{-1}$	$-0{\cdot}18194 \times 10^{-2}$	$0{\cdot}17337 \times 10^{-5}$	$-0{\cdot}25957 \times 10^{-1}$
$0{\cdot}70 \times 10^{0}$	$-0{\cdot}16485 \times 10^{-2}$	$0{\cdot}12288 \times 10^{-5}$	$-0{\cdot}15660 \times 10^{-1}$	$-0{\cdot}16688 \times 10^{-2}$	$0{\cdot}17982 \times 10^{-5}$	$-0{\cdot}14771 \times 10^{-1}$
$0{\cdot}80 \times 10^{0}$	$-0{\cdot}12556 \times 10^{-2}$	$0{\cdot}97040 \times 10^{-6}$	$-0{\cdot}11049 \times 10^{-1}$	$-0{\cdot}15411 \times 10^{-2}$	$0{\cdot}18283 \times 10^{-5}$	$-0{\cdot}71933 \times 10^{-2}$
$0{\cdot}90 \times 10^{0}$	$-0{\cdot}93801 \times 10^{-3}$	$0{\cdot}71983 \times 10^{-6}$	$-0{\cdot}74709 \times 10^{-2}$	$-0{\cdot}13755 \times 10^{-2}$	$0{\cdot}17241 \times 10^{-5}$	$-0{\cdot}20024 \times 10^{-2}$
$0{\cdot}10 \times 10^{1}$	$-0{\cdot}69918 \times 10^{-3}$	$0{\cdot}78136 \times 10^{-6}$	$-0{\cdot}56817 \times 10^{-2}$	$-0{\cdot}11904 \times 10^{-2}$	$0{\cdot}16010 \times 10^{-5}$	$0{\cdot}14540 \times 10^{-2}$
$0{\cdot}20 \times 10^{1}$	$0{\cdot}16240 \times 10^{-3}$	$-0{\cdot}95263 \times 10^{-6}$	$-0{\cdot}29422 \times 10^{-2}$	$-0{\cdot}37972 \times 10^{-4}$	$0{\cdot}15680 \times 10^{-7}$	$-0{\cdot}17536 \times 10^{-2}$
$0{\cdot}30 \times 10^{1}$	$0{\cdot}35601 \times 10^{-4}$	$0{\cdot}32540 \times 10^{-6}$	$-0{\cdot}39796 \times 10^{-3}$	$0{\cdot}33088 \times 10^{-4}$	$0{\cdot}57355 \times 10^{-6}$	$-0{\cdot}47155 \times 10^{-2}$
$0{\cdot}40 \times 10^{1}$	$-0{\cdot}18539 \times 10^{-4}$	$-0{\cdot}21952 \times 10^{-7}$	$-0{\cdot}10979 \times 10^{-2}$	$-0{\cdot}32885 \times 10^{-3}$	$0{\cdot}87351 \times 10^{-6}$	$-0{\cdot}72666 \times 10^{-3}$
$0{\cdot}50 \times 10^{1}$	$0{\cdot}45689 \times 10^{-5}$	$-0{\cdot}28684 \times 10^{-8}$	$-0{\cdot}74403 \times 10^{-3}$	$-0{\cdot}25442 \times 10^{-3}$	$-0{\cdot}34262 \times 10^{-6}$	$0{\cdot}34080 \times 10^{-2}$
$0{\cdot}60 \times 10^{1}$	$0{\cdot}59220 \times 10^{-5}$	$-0{\cdot}43428 \times 10^{-8}$	$-0{\cdot}62884 \times 10^{-3}$	$0{\cdot}57105 \times 10^{-3}$	$-0{\cdot}41076 \times 10^{-6}$	$0{\cdot}10757 \times 10^{-2}$
$0{\cdot}70 \times 10^{1}$	$-0{\cdot}97853 \times 10^{-6}$	$-0{\cdot}54317 \times 10^{-10}$	$-0{\cdot}55631 \times 10^{-3}$	$-0{\cdot}17357 \times 10^{-3}$	$-0{\cdot}74109 \times 10^{-7}$	$0{\cdot}17315 \times 10^{-2}$
$0{\cdot}80 \times 10^{1}$	$-0{\cdot}48870 \times 10^{-5}$	$0{\cdot}34993 \times 10^{-10}$	$-0{\cdot}51561 \times 10^{-3}$	$0{\cdot}13661 \times 10^{-4}$	$-0{\cdot}23097 \times 10^{-8}$	$0{\cdot}15175 \times 10^{-2}$
$0{\cdot}90 \times 10^{1}$	$-0{\cdot}56519 \times 10^{-5}$	$0{\cdot}50447 \times 10^{-9}$	$-0{\cdot}25615 \times 10^{-3}$	$0{\cdot}30732 \times 10^{-4}$	$-0{\cdot}54931 \times 10^{-8}$	$0{\cdot}80143 \times 10^{-3}$
$0{\cdot}10 \times 10^{2}$	$0{\cdot}73536 \times 10^{-6}$	$0{\cdot}10674 \times 10^{-8}$	$-0{\cdot}13273 \times 10^{-3}$	$0{\cdot}26498 \times 10^{-4}$	$0{\cdot}25694 \times 10^{-7}$	$-0{\cdot}48359 \times 10^{-4}$

length $x = 2$, but the shapes for $x < 2$ are slightly different. The jet swell ratio predicted by the finite difference method is lower than that by the finite element method.

The effect of surface tension on the jet free surface for $Re = 1$ is shown in Figure 6; since $C_0 > 1$, the jet swells after emanating from the slot. As the surface tension increases, Ca will decrease and the jet will have less swelling, even though the effect is not significant. Similar results for moderate Re are given in Figure 7. Comparing with the jet shapes in Figure 6, the jet contracts now instead of swelling and the fluid surface tension tends to reduce the contraction. The jet will contract as the fluid inertia or the Reynolds number increases. The effect of the surface tension on the jet shape appears to be less important as Re increases. With $Re = 100$ the effect of Ca on the jet surface is not detectable; the curve of $Ca = 0{\cdot}5$ coincides with curve (1) and is not shown in Figure 7. More detailed results regarding the effect of surface tension can be found in Omodei[9] and Georgiou *et al.*[4]

We also computed the errors in the mass conservation equation (1) and the tangential and normal stress balance equations (15b) and (15c) on the jet free surface. If these three equations are exactly satisfied, the right-hand sides of these equations should be zero. Once the flow field is determined, the left-hand sides of these equations can be approximated and $\bar{D}$, Ts and Tn denote the residuals of these three equations respectively. Table II presents a comparison of these errors with the works of Omodei[9] and Dutta and Ryan.[1] Omodei did not provide data on mass conservation errors, therefore only Ts and Tn from his work are listed here. It is noted that Ts and Tn are small for the three approaches. Comparing with the work of Dutta and Ryan, the errors of mass conservation for the present study are smaller but the values of Ts on the first few grid points are slightly higher. Values of Tn, Ts and $\bar{D}$ all decrease as x increases and become negligible if $x > 2$.

The effects of Re on these errors are given in Table III. When Re is small, the errors are only significant for several downstream mesh points close to the separation point and are negligible for downstream points far from the separation point; but the errors will not decrease on the free surface when Re is large. Reducing Ca, as indicated by the results in Table IV, seems to have little effect on these errors.

CONCLUSIONS

We have developed a finite difference technique to study the Newtonian jet swell problem. The mathematical problem of the jet swelling is formulated with the streamfunction and vorticity as dependent variables. The boundary-fitted co-ordinate transformation method developed by Thompson *et al.*[6,7] was adopted to map the flow geometry into a rectangle, and the flow equations are solved in the transformed plane. The iteration of the free surface is similar to the approach of Dutta and Ryan,[1] but we have used an adjustable parameter for free-surface iterations. With this modificaton we could obtain convergent solutions for the Reynolds number as high as 100. Comparing with the existing results based on finite element simulations, the jet swell ratio we computed is slightly lower, but the differences are within 5%.

We also computed the errors on mass conservation and tangential and normal stress balances on the jet free surface. When Re is small, the errors are only significant on the first few points near the separation point. However, when Re is large, the errors will remain on the jet surface from the separation point to a distance far downstream.

At the present time, even though the finite element method can simulate the jet flow problem over wider ranges of Reynolds numbers and capillary numbers than can the finite difference method, the application of numerical mapping is capable of locating the jet free surface

successfully, and it deserves further investigation so that the range of convergence may be extended. For example, the standard central difference scheme may be replaced by other finite difference schemes to discretize the inertial terms in the flow equations; a study on this subject is under way.

ACKNOWLEDGEMENT

This research was supported by the National Research Council, Republic of China.

APPENDIX: NOTATION

$\bar{A}$	a constant, equation (35)
a	one-half of the slot gap
Ca	capillary number, $\mu\langle u\rangle/\sigma$
C_0	jet swell ratio, δ/a
$\bar{D}$	error of mass conservation
f	a function in the transformed plane
h, H	location of the free surface, dimensional and dimensionless
I, J	numbers of grid points in the transformed plane
k	adjustable parameter, equation (34)
M, N	forcing functions for mapping, equation (16)
$\bar{p}, p$	fluid pressure, dimensional and dimensionless
p_a	surrounding pressure
$\bar{R}, R$	curvature of the jet surface, dimensional and dimensionless
Re	Reynolds number, $\rho\langle u\rangle a/\mu$
r, s	mesh intervals in the transformed plane
$\bar{S}$	a surface tension parameter, $\bar{S}\equiv Ca/Re$
Tn	error of normal stress balance
Ts	error of tangential stress balance
$\bar{u}, u$	velocity component in the x-direction, dimensional and dimensionless
u_0	uniform downstream jet velocity
$\langle u\rangle$	average fluid speed upstream in the slot
$\bar{v}, v$	velocity component in the y-direction, dimensional and dimensionless
$\bar{x}, \bar{y}; x, y$	Cartesian co-ordinates, dimensional and dimensionless

Greek letters

α, β, γ	coefficients of mapping equations, equation (16c)
δ	one-half of the final jet thickness
δ_0	a parameter, equation (35)
λ	Jacobian of mapping equation, equation (16c)
μ	fluid viscosity
ξ, η	co-ordinates in the transformed plane
ρ	fluid density
σ	surface tension coefficient
$\bar{\varphi}, \varphi$	streamfunction, dimensional and dimensionless
$\bar{\omega}, \omega$	vorticity, dimensional and dimensionless

Subscripts

ξ, η	partial differentiation
i, j	indices

REFERENCES

1. A. Dutta and M. E. Ryan, 'Dynamics of a creeping Newtonian jet with gravity and surface tension: a finite difference technique for solving steady free-surface flows using orthogonal curvilinear coordinates', *AIChE J.*, **28**, 220–232 (1982).
2. R. I. Tanner, *Engineering Rheology*, Clarendon Press, Oxford, 1988.
3. S. F. Kistler, 'The fluid mechanics of curtain coating and related viscous free surface flow', *Ph.D. Thesis*, University of Minnesota, 1983.
4. G. C. Georgiou, T. C. Papanastasiou and J. O. Wilkes, 'Laminar Newtonian jets at high Reynolds number and high surface tension', *AIChE J.*, **34**, 1559–1562 (1988).
5. M. J. Crochet, A. R. Davis and K. Walters, *Numerical Simulation of Non-Newtonian Flow*, Elsevier, Amsterdam, 1984.
6. J. F. Thompson, F. C. Thomas and C. W. Mastin, 'Automatic numerical generation of body-fitted curvilinear coordinate system for field containing any number of arbitrary two-dimensional bodies', *J. Comput. Phys.*, **15**, 299–319 (1974).
7. J. F. Thompson, Z. U. A. Warsi and C. W. Mastin, 'Boundary-fitted coordinate systems for numerical solution of partial differential equations—a review', *J. Comput. Phys.*, **47**, 1–108 (1982).
8. S. Richardson, 'A "stick–slip" problem related to the motion of a free jet at low Reynolds number', *Proc. Camb. Phil. Soc.*, **67**, 477–487 (1970).
9. B. J. Omodei, 'Computer solutions of a plane Newtonian jet with surface tension', *Comput. Fluids*, **7**, 79–96 (1979).
10. K. J. Ruschak, 'A method for incorporating free boundary with surface tension in finite-element fluid-flow simulators', *Int. j. numer. methods eng.*, **15**, 639–648 (1980).
11. P. J. Roache, *Computational Fluid Dynamics*, Hermosa, Albuquerque, NM, 1972.
12. R. Peyret and T. D. Taylor, *Computational Methods for Fluid Flow*, Springer, New York, 1983.